



Fabrication of monodispersed nickel flower-like architectures via a solvent-thermal process and analysis of their magnetic and electromagnetic properties

Jing Kong^a, Wei Liu^{b,*}, Fenglong Wang^a, Xinzhen Wang^a, Liqiang Luan^b, Jiurong Liu^{a,**}, Yuan Wang^a, Zijun Zhang^a, Masahiro Itoh^c, Ken-ichi Machida^c

^a Key Laboratory for Liquid–Solid Structural Evolution and Processing of Materials, Ministry of Education and School of Materials Science and Engineering, Shandong University, Jinan 250061, People's Republic of China

^b State Key Laboratory of Crystal Materials, Shandong University, Jinan 250100, People's Republic of China

^c Center for Advanced Science and Innovation, Osaka University, 2-1 Yamadaoka, Suita, Osaka 565-0871, Japan

ARTICLE INFO

Article history:

Received 2 June 2011

Received in revised form

8 September 2011

Accepted 14 September 2011

Available online 17 September 2011

Keywords:

Nickel flower-like architecture

Solvent-thermal

Nanoflake

Anisotropic field

Electromagnetic wave absorption

ABSTRACT

Monodispersed Ni flower-like architectures with size of 1–2 μm were synthesized through a facile solvent-thermal process in 1,2-propanediol solution in the presence of polyethylene glycol (PEG) and sodium alkali for electromagnetic absorption application. The Ni architectures are composed of nanoflakes, which assemble to form three dimensional flower-like structure, and the thickness of nanoflakes is about 10–40 nm. A possible formation mechanism for Ni flower-like architectures was proposed and it was confirmed by the control experiments. The Ni architectures exhibited a saturation magnetization (M_s) of 47.7 emu/g and a large coercivity (H_{c1}) of 332.3 Oe. The epoxy resin composites with 20 vol% Ni sample provided good electromagnetic wave absorption performance (reflection loss < -20 dB) in the range of 2.8–6.3 GHz over absorber thickness of 2.6–5.0 mm.

© 2011 Elsevier Inc. All rights reserved.

1. Introduction

The recent researches in nanotechnology have witnessed an increasing trend toward fabrication of nanoscale inorganic materials with one-, two-, and three-dimensional (3D) structures, owing to their shape-property correlation that has been revealed in various fields [1–6]. Novel 3D nano/micro-structures constructed by low-dimensional nanoscale building blocks, such as nanoparticles, nanocones, nanorods, nanoribbons, etc., have attracted extensive attentions, because complex structures with anisotropic assembly are believed to exhibit unusual properties and may have potential applications as future nano/micro-devices [7–10]. As a “bottom-up” synthesis approach, the solution-based procedures have been proved effective in simple fabrication of self-assembled 3D architectures because of their potential to allow for precise control over the morphology and size of architectures [11]. Self-assembled 3D flower-like hierarchical β -Ni(OH)₂ hollow architectures composed of nanosheets were synthesized by Zhu et al. via the stepwise growth and Ostwald

ripening in a facile hydrothermal condition [12]. Liu et al. synthesized flower-like Ni–Fe alloy nanostructures with an anisotropic growth of nanorods along their easy magnetic axis under kinetic control [13]. Narayanaswamy et al. also reported that ZnO, MnO or CoO nanocrystals assembled to form flower-like structures in a common crystallographic orientation [14]. The stable 3D flower-like structures can offer potential applications for the development of high performance electronic, optoelectronic, and sensing devices.

In addition to being utilized as catalyst, magnetic recording media, medical diagnosis, and electrode [15–17], nickel nano/micro-structures as electromagnetic (EM) wave absorption materials have drawn extensive research attention with the ever-accelerated development of wireless communications and high frequency circuit devices. Recently, different nickel based nano/micro-structures such as nanospheres, urchinlike chains, branched nanowires, polyaniline coated Ni, and carbon coated Ni nanocapsules have been synthesized and their EM wave absorption has also been investigated in GHz range [18–25]. The experimental results indicated that the EM absorption characteristics, i.e., frequency, thickness, and absorbing band-width are strongly related to Ni micro-structures. Wang et al. synthesized nickel nanomaterials with different morphologies including superfine nanoparticles, rings, smooth chains, and urchinlike

* Corresponding author.

** Corresponding author. Fax: +86 531 88392315.

E-mail addresses: jrlu@sdu.edu.cn (W. Liu), weiliu@sdu.edu.cn (J. Liu).

chains by adjusting the reaction conditions [20]. Urchinlike nickel chains showed more effective EM absorption in contrast with other structures mainly due to the large aspect ratio of the aciculae on the nickel chain surface. The incident EM wave will be multi-scattered in the presence of aciculae resulting in repeated absorption just as the wall in an EM wave darkroom consisting of cone-shaped absorbers. EM absorption properties of aloe-like nickel flowers assembled on hollow glass spheres have also been investigated [26], but the material only gave weak absorption ($RL > -20$ dB) in GHz range because the addition of non-magnetic component decreased the saturation magnetization (M_s) of the composites thus affecting its EM absorption. The above results suggest that pure nickel 3D flower-like nano/microstructures will probably provide more efficient EM wave absorption due to their high M_s , large aspect ratio of flake-like petal and large surface area. To the best of our knowledge, few contributions have been presented exploring Ni flower-like nano/microstructures composed of nanoflakes as EM absorption materials.

Wet chemical procedures exploring hydrazine as reducing agent have been widely investigated to synthesize Ni flower-like structures assembling from nanocones, swordlike petals, or columns made up of aligned nanoplates [27–30]. In the above works, the oriented growth of Ni building blocks intensively relies on the mediated surfactant or structure-directing agent. However, the assembled nanostructures are not monodispersed or have broad size distribution, which will affect their practical applications. In surfactant-free synthesis method, flower-like Ni nanostructures could be obtained under a rotating magnetic field [31], but this approach usually suffers from high cost and complicated operation. Bai et al. also fabricated Ni flower-like clusters composed of nanoflakes employing glycol as both solvent and reducing agent [32], however, the flower-like structures with broad size distribution are not apparent. More recently, Guan's group also synthesized Ni flower-like nanostructure through a polyol reduction process without any surfactant. The introduction of water to the polyol system plays a key role in the formation of the flower-like nanostructure although the exact reaction mechanism is not clear. In this synthesis process, the addition amount of water needs to be precisely controlled and long reaction time (12 h) is necessary [33].

Herein, we report a novel facile solvent-thermal approach to fabricate monodispersed flower-like Ni architectures, in which 1,2-propanediol was employed as solvent and reducing agent with the assistance of sodium alkali. Through controlling the growth rate, 2D building blocks (nanoflakes) were obtained due to the oriented growth of Ni crystallites along crystallographically specific direction. A possible formation mechanism was proposed based on a series of control experiments. The magnetic and EM wave absorption properties of the monodispersed flower-like Ni architectures were investigated.

2. Experimental details

2.1. Synthesis of monodispersed Ni flower-like architectures

Tetrahydrated nickel acetate ($\text{Ni}(\text{CH}_3\text{COO})_2 \cdot 4\text{H}_2\text{O}$), polyethylene glycol (PEG), 1,2-propanediol, sodium chloride (NaCl), and sodium alkali (NaOH) were purchased from Sinopharm Chemical Reagent Co., Ltd. All reactants were of analytical grade and used as received without any further purification.

The monodispersed Ni flower-like architectures were synthesized by a facile one-pot solvent-thermal reduction process. Typically, 1 g polyethylene glycol (PEG) was dissolved in 40 mL 1,2-propanediol, followed by the addition of 2.5 g tetrahydrated nickel acetate ($\text{Ni}(\text{CH}_3\text{COO})_2 \cdot 4\text{H}_2\text{O}$) and 1 g NaCl under magnetic

stirring. The green solution became purple emulsion with the addition of 2 M sodium alkali. After magnetic stirring for 1 h, the purple emulsion was transferred into a 60 mL Teflon-lined autoclave, and subsequently sealed and heated at 443 K for 3 h in an oven. The black product was centrifuged and washed with deionized water and ethanol for five times, respectively, and then dried under vacuum overnight for further characterization. To investigate the formation mechanism of the flower-like architectures, we carried out a series of experiments by varying the reaction time and the addition amount of sodium alkali and PEG.

2.2. Characterization

X-ray diffraction (XRD) pattern was obtained by a Rigaku Dmax-rc X-ray diffractometer with Ni filter $\text{CuK}\alpha$ radiation ($V=40$ kV, $I=50$ mA) at a scanning rate of $4^\circ/\text{min}$. The microstructures of the resultant products were examined using a JSM-6700F field emission scanning electron microscope (FE-SEM) at an accelerating voltage of 20 kV and electric current of 1.0×10^{-10} A, and a Hitachi H-800 transmission electron microscope (TEM) at an accelerating voltage of 150 kV. To measure the relative permeability (μ_r) and permittivity (ϵ_r) values, epoxy resin composites were prepared by homogeneously mixing epoxy resin with 20 vol% Ni flower-like powders and compressing into cylindrical-shaped compacts. After cured at 333 K for 60 min, these compacts were cut into toroidal-shaped samples with outer diameter of 7.00 mm and inner diameter of 3.04 mm. The measurements were carried out with a vector network analyzer (Agilent Technologies E8363A) in the range of 0.05–18.05 GHz. The frequency dependence of reflection loss (RL) was calculated from the measured μ_r and ϵ_r at the given frequency and absorber thickness.

3. Results and discussion

3.1. Structure and morphology

The phase and purity of the as-synthesized nickel flower-like architectures was investigated by XRD. The characteristic peaks of XRD pattern (Fig. 1(a)) could match well with face-centered cubic (fcc) nickel (JCPDS 04-0850), and no peak of any other phase is detected indicating that pure nickel flower-like architectures have been prepared in this solvent-thermal process. In addition, we found that the peak intensity of (111) face is much stronger than the normal level. The FE-SEM and TEM images provide further insight into the structure and morphology of the as-synthesized nickel architectures. From the panoramic SEM image (Fig. 1(b)), Ni formed flower-like architectures with size of 1.0–2.0 μm . Close inspection reveals that the nickel architectures are built of nanoflakes, which intersect with each other in the center to form the three dimensional flower-like structures (Fig. 1(c)), and the thickness of nanoflake is ca. 10–40 nm. The prepared architectures are very stable, and even two hours of ultrasonication cannot break them into discrete flakes, indicating that the flower-like architectures are integrative. The TEM image (Fig. 1(d)) shows that the obtained flower-like structures have a solid interior core with nanoflakes growing on it. By aligning the electron beam perpendicular to one nanoflake, the selected area electron diffraction (SAED) pattern (inset of Fig. 1(d)) reveals the single crystalline nature of the nanoflake. In the SAED pattern, six-fold symmetry near the center could be indexed to {220} diffractions of fcc nickel, which suggests that the electron beam was along the [111] zone axis of the fcc crystal structure [29]. The highly oriented diffraction spots indicate that the surface of two-dimensional (2D) flake is the (111) plane, which is in good

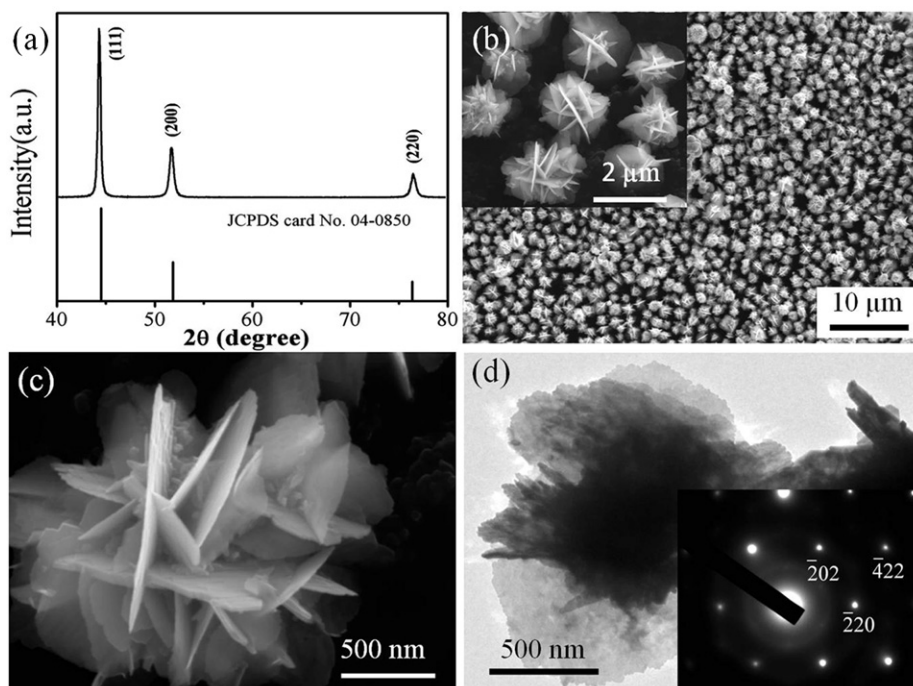


Fig. 1. XRD pattern (a), SEM (b, c), and TEM (d) images of the as-obtained Ni flower-like architectures. The inset of (d) is SAED pattern of an individual nanoflake.

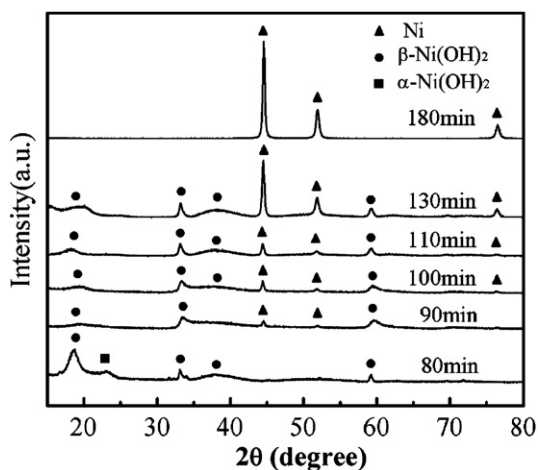


Fig. 2. XRD patterns of samples reacted at 443 K for different times.

agreement with the rather strong diffraction peak of (1 1 1) in the XRD pattern.

3.2. Formation mechanism

In order to gain insight into the formation mechanism of the flower-like nickel architectures, time-dependent experiments were performed. The morphology and phase of products were studied by SEM, TEM, and XRD measurements. After 80 min, a green suspension was obtained, and the XRD pattern (Fig. 2) presents the characteristic of poorly crystallized Ni(OH)₂ without any shaped particle (Fig. 3(a)). Generally, Ni(OH)₂ has two different phases: α phase and β phase. α phase, which is a metastable phase, can be spontaneously transformed to β phase in strong alkaline condition [33]. The diffraction peaks could be mainly indexed to β -Ni(OH)₂ after 80 min reaction, while a weak diffraction peak ($2\theta=23^\circ$) is assigned to the (006) plane of α phase, which disappeared with increasing the reaction time.

When proceeded for 90 min, the weak diffraction peaks assigned to fcc Ni phase appeared, indicating that the reduction of Ni(OH)₂ intermediate began to occur. At the same time, a few small nanoparticles with size less than 400 nm were observed on the SEM image (Fig. 3(b)). Increasing the reaction time to 100 min, the intensity of the diffraction peaks of fcc Ni increased and a lot of nanoparticles less than 1 μ m with smooth surface formed as shown in Fig. 3(c) and (d). When the reaction was continued for 110 min, plenty of spheres with relatively rough surface full of thin slices could be observed (Fig. 3(e) and (f)), suggesting that the flower-like structure began to form at the current time. Further prolonging the reaction time to 130 min, the intensity of diffraction peaks of fcc Ni (Fig. 2) increased drastically indicating that most of Ni(OH)₂ intermediate has been reduced to Ni, meanwhile, the surface became more rough with the growth of flower-like structure (Fig. 3(g) and (h)). When the reaction was maintained for 180 min, all peaks of XRD pattern could be assigned to fcc Ni and more homogeneous well-defined flower-like architectures with smooth nanoflakes were prepared (Fig. 1). Therefore, the growth of flower-like architectures involves the evolution processes containing nucleation of crystallites, aggregation of initial crystallites, growth of slices, and re-crystallization of primary building units.

On the basis of the investigation and analysis above, the possible formation mechanism of nickel flower-like architectures was proposed in Fig. 4. Firstly, Ni(OH)₂ with poor crystallization was produced through the reaction among the raw materials. With the progress of reaction, the original Ni(OH)₂ intermediate nucleated to form nanoparticles, and the tiny particles agglomerate into larger spheres to reduce the surface energy. In this solvent-thermal synthesis, 1,2-propanediol is used as solvent and reducing agent for Ni²⁺. It initially dehydrates to produce propionaldehyde and then reacts with Ni²⁺ generated from Ni(OH)₂ intermediate to form primary Ni atoms [34,35]. Following the aggregation of nanoparticles into spheres, the number of free Ni²⁺ ions released from Ni(OH)₂ in solution reduced a lot; thereafter, relatively small thin slices grew slowly since the Ni atoms will preferentially adsorb and bond to the active sites of

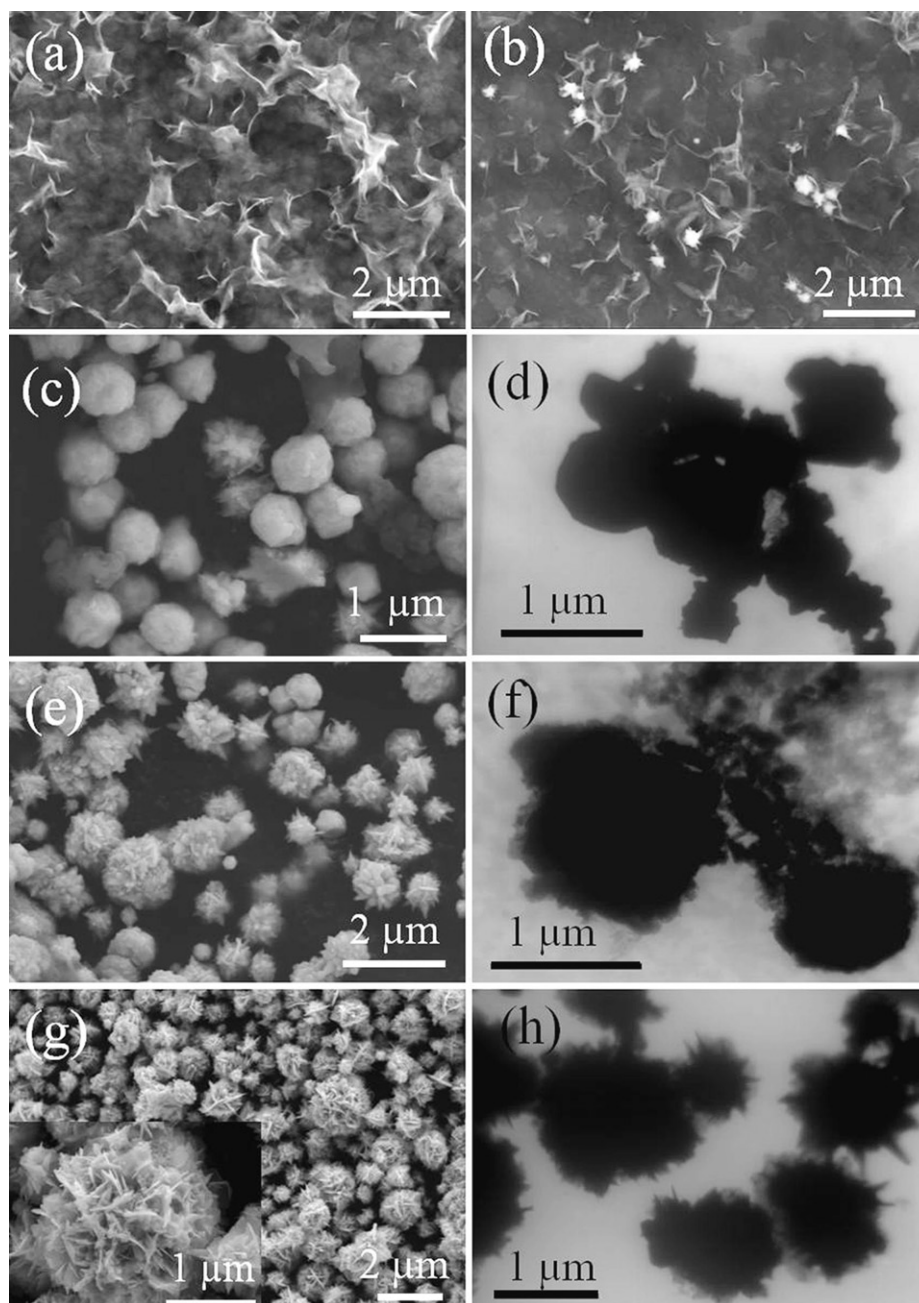


Fig. 3. SEM and TEM images of samples reacted at 443 K for times of the following: (a) 80 min, (b) 90 min, (c, d) 100 min, (e, f) 110 min, and (g, h) 130 min.

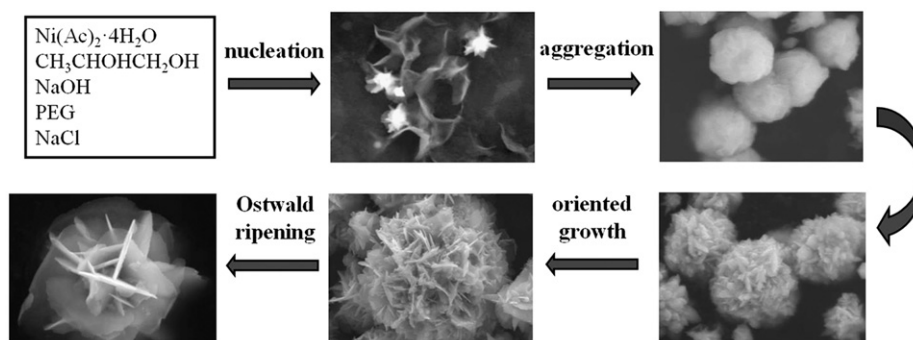


Fig. 4. Schematic for the formation mechanism of Ni flower-like architectures.

small protuberances (shown in Fig. 3(e) and (f)), which have relatively higher free energy on the sphere surface [28]. Crystal faces with high surface energy exhibit the fastest growth rate and are minimized or even disappear in the final morphology [36]. Wulff's rule [37] illustrates the equilibrium morphology of a crystal as being given by the minimum surface energy of all exposed crystal faces and this thermodynamic model can be used to explain the oriented growth of slices in this synthesis process. In the current system, the crystalline growth of slices is preferentially along the $\langle 110 \rangle$ or $\langle 100 \rangle$ direction, forming the top/bottom faces of $\{111\}$ planes with the lowest surface energy for Ni fcc crystal structure [30]. The similar anisotropic growth to 2D crystal nanosheets has also been observed in other fcc materials [38,39]. Finally, the flower-like nickel architectures comprised of single-crystal flakes formed through oriented growth of slices at the expense of adjacent smaller slices/nanoparticles and the metastable crystallites in the solid interior core, which can be referred to the Ostwald ripening process [40,41]. In the ripening process, larger flakes with a relative small surface energy are thermodynamically favored and the unstable tiny crystals dissolved to provide the source material for the growth of flakes during the dissolution and recrystallization process. Specifically, the dissolved nickel atoms may continuously attach and bond to the surface of larger flakes, and spread the $\{111\}$ planes in order to achieve a minimum total free energy [42].

3.3. Effects of reaction conditions

Usually, the final morphology of Ni structures prepared via wet chemical procedures without template agent is correlated with temperature, reaction time, reducing agent, surfactant, etc. [27–29]. In this work, only a small amount of $\text{Ni}(\text{OH})_2$ was reduced to Ni when the hydrothermal reaction temperature decreased to 433 K after 3 h reaction. If the reaction temperature is higher than 443 K, the size of Ni flower-like architectures will increase with the temperature enhancement. Besides the time-dependent morphology evolution in the formation of nickel flower-like architectures, time prolonged experiments were also carried out. When the reaction was maintained for 24 h, there was no obvious change in the morphology of flower-like architectures in addition to a slight increase in the particle size (ca. $2 \mu\text{m}$) and a curling tendency of the nanoflakes (see Fig. S1). The microstructure and size had no variation when the reaction time was further increased to 48 h in comparison with the sample produced after 24 h reaction (SEM images not shown). In addition, it was found that sodium alkali played an important role in the formation of Ni morphology feature. SEM images in Fig. 5 show the typical morphologies of three samples obtained at different sodium alkali concentration, whilst the other experimental parameters were kept. If the NaOH concentration was less than 0.8 M, pure metallic Ni could not be obtained suggesting that NaOH acts as the assisting agent to enhance the reducing ability of polyol [43,44]. When the addition quantity of NaOH was 1 M, only two or three nanoflakes intersected with each other to form the Ni flower-like structure and a lot of nanoparticles were

observed (Fig. 5(a)). With the NaOH concentration increasing to 1.5 M, the quantity of nanoflakes constituting one nickel flower increased, nevertheless, the nanoparticles with diameter of ca. 200 nm still existed (Fig. 5(b)). When 4 M NaOH was added to the solution, the Ni architectures ($1.0\text{--}3.0 \mu\text{m}$) with prickly surface composed of short nanoplates with the thickness of 30–60 nm were prepared as shown in Fig. 5(c). Our experimental results confirmed that the increase of alkali concentration could improve the reducing ability of 1,2-propanediol. The deposition rate is accelerated with increasing NaOH concentration enhancing the nucleation and crystal growth of Ni, which kinetically affects the formation of Ni architectures, and thus the Ni morphology can be controlled by varying NaOH concentration in the reaction. In this study, the well-defined Ni flower-like architectures with smooth flakes were obtained with the concentration of NaOH at 2 M.

PEG, a kind of nonionic surfactant, has been widely used to facilitate the preparation of monodispersed nano/micro-particles [45,46]. In order to investigate the effect of PEG on the final morphology, the control experiment was performed in the absence of PEG. Experimental results showed that monodispersed Ni flower-like structures were not obtained in addition to a lot of particles with a wide size distribution (Fig. 6). When the PEG addition amount increased to 2 g, flower-like Ni architectures with larger size of ca. $2\text{--}3 \mu\text{m}$ formed, and the quantity of nanoflakes constituting one nickel flower increased (shown in Fig. S2). It is believed that PEG plays an important role as the surface modifier for the formation of flower-like structures. PEG physically adsorbed on the $\{111\}$ planes of Ni subunits can inhibit the growth of $\{111\}$ planes resulting in the oriented growth of nanoflakes during the reaction process. Xu et al. also reported the 3D NiS flower-like architectures assembled from the sheet-like primary crystals with the assistance of PEG as the morphology-directing reagent [47].

In this study, we also found that the morphology of final product depends on the addition of NaCl. The messy clusters of nanoflakes with no shaped feature were obtained without NaCl addition (see Fig. S3), while the well-defined Ni flower-like architectures with smooth flakes generated when 1 g NaCl was added to the reaction. Previous investigations confirmed that the

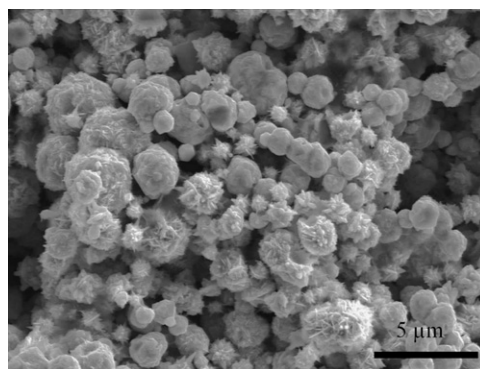


Fig. 6. SEM image of sample prepared at 443 K for 3 h with no PEG addition.

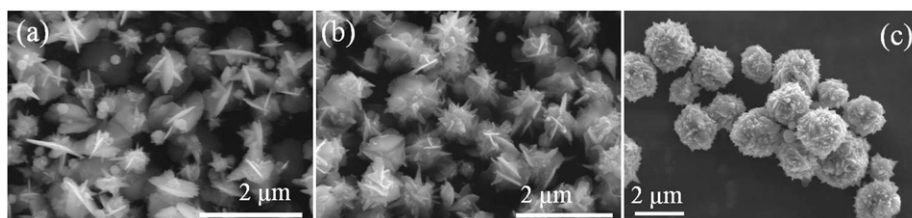


Fig. 5. SEM images of samples produced at 443 K for 3 h with different NaOH concentration (a) 1 M, (b) 1.5 M, and (c) 4 M.

inorganic soluble salts as complexing agent added in solution can inhibit the deposition of crystallites [48,49], and therefore, the deposition rate of Ni decreased through the addition of NaCl in favor of the growth of monodispersed flower-like structures due to the strong coordination of Cl^- to Ni^{2+} in this reaction system.

3.4. Magnetic property

It is well known that the magnetic properties of nanomaterials are affected by their size and morphology. Fig. 7 shows the typical magnetization hysteresis (M–H) loops of nickel flower-like architectures measured at room temperature. The sample showed saturation magnetization (M_s) of 47.7 emu/g, coercivity (H_{cj}) of 332.3 Oe, and remnant magnetization (M_r) of 15.4 emu/g. The measured M_s value of nickel flower-like architectures is lower than that of bulk Ni ($M_s=55.9$ emu/g) [31]. The decrease of M_s is probably attributed to the existence of non-magnetic or weak magnetic Ni oxide shell due to the exposure of sample in air after synthesis. Moreover, the flower-like architectures have large surface area, which induced the enhancement of spin disorder on the surface [20], might be another reason for the decrease of M_s . However, the coercivity is much higher than that of the bulk nickel (ca. 0.7 Oe) [31], mainly resulting from the enhanced shape anisotropy of nickel nanoflakes [21]. As mentioned above, the flower-like architectures are composed of nickel nanoflakes, which were obtained by the anisotropic growth of Ni increasing the aspect ratio (Fig. 1(c)). Generally, the magnetocrystalline anisotropy and the shape anisotropy of materials contribute to coercivity. In this work, the shape anisotropy increased due to the high aspect ratio of Ni nanoflakes [50], which leads to a higher coercivity comparing with other Ni nano/micro-structures [20,26,51].

3.5. EM wave absorption properties

Magnetic powders dispersed in nonconductive matrix, such as resin or rubber, are favorable to EM wave absorption materials since it is facile to prepare lightweight absorbers with a remarkable flexibility in combining with various EM wave devices. Fig. 8(a) shows that the real part (ϵ') and imaginary part (ϵ'') of relative permittivity for the resin composites with 20 vol% nickel flower-like sample were low and almost independent of frequency between 1.0 and 8.0 GHz, for which the relative permittivity ($\epsilon_r = \epsilon_r' - j\epsilon_r''$) showed less variation ($\epsilon_r' \sim 16$ and $\epsilon_r'' \sim 2$). The dispersive permittivity behavior can be attributed to the decrease of electric conductivity and space-charge polarization between Ni powders isolated by epoxy resin efficiently.

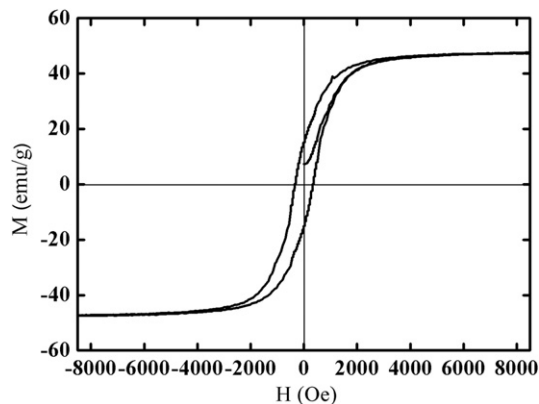


Fig. 7. Hysteresis loop of the Ni flower-like architectures measured at room temperature.

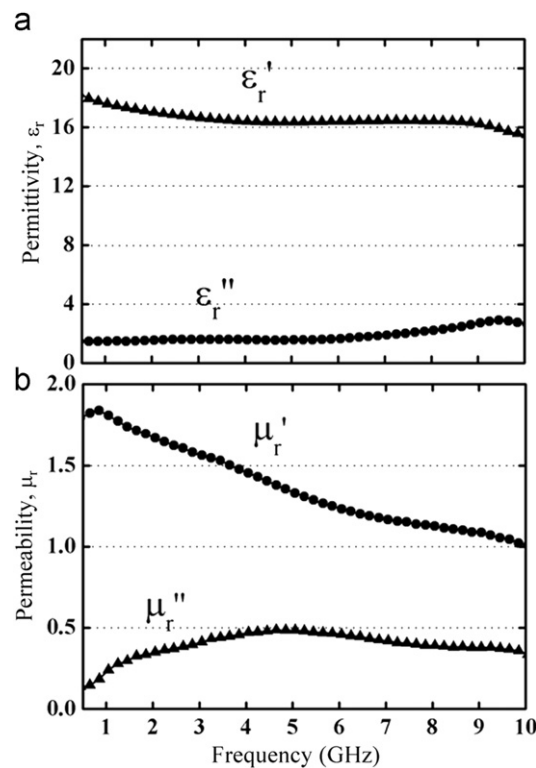


Fig. 8. Relative permittivity ϵ_r (a) and permeability μ_r (b) curves plotted against frequency for the resin composites with 20 vol% Ni flower-like architectures in the 0.05–10.0 GHz range.

Fig. 8(b) shows the frequency dependences of the relative permeability for the resin composites containing 20 vol% Ni flower-like powders. The real part of relative permeability (μ_r') declined from 1.7 to 1.0 with frequency in the 0.5–10.0 GHz range, while the imaginary part of relative permeability (μ_r'') increased from 0.1 to 0.49 over a range of 0.5–5.0 GHz, and then decreased gradually in the higher frequency range. The μ_r'' curve exhibited a peak in a broad frequency range (2.0–10.0 GHz) with a maximum point at 4.8 GHz. The magnetic loss peak at 4.8 GHz can be ascribed to the natural resonance of Ni flower-like architectures [18,22]. Comparing with the fcc bulk Ni (several tens of megahertz) [19], the natural resonance frequency shifted to higher GHz range. According to the ferromagnetic resonance theory [52], the natural resonance frequency linearly varying with the anisotropy field can be expressed by the equation: $2\pi f_r = rH_{\text{eff}}$, where r is the gyromagnetic ratio, and H_{eff} is the effective anisotropy field. Deng et al. [53] proposed using H_{cj} to replace H_{eff} considering that it is difficult to calculate H_{eff} for magnetic materials with nanostructures since magnetocrystalline anisotropy, particle geometry, particle size, and magnetic interaction of particles all contribute to H_{eff} . In this study, the measured H_{cj} (332.3 Oe) of Ni flower-like architectures is much higher than that of the bulk nickel, therefore, the natural resonance frequency shifted from several tens of megahertz to 4.8 GHz. The same natural resonance frequency enhancements have also been observed for cobalt nanoflakes, iron submicron cubes, and Ni nanowires attributing to the increase of shape anisotropy [21,50,54].

To further reveal the EM wave absorption properties, the reflection loss (RL) curves were calculated from the measured relative permeability and permittivity at the given frequency and absorber thickness according to the following equations [55,56]:

$$Z_{in} = Z_0(\mu_r/\epsilon_r)^{1/2} \tanh\{j(2\pi f d/c)(\mu_r\epsilon_r)^{1/2}\} \quad (1)$$

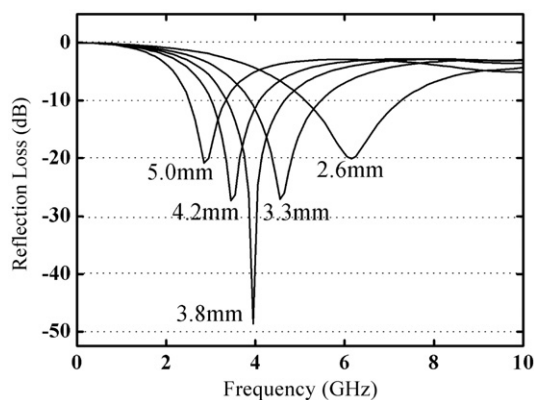


Fig. 9. Frequency dependences of the reflection loss (RL) for the resin composites with 20 vol% Ni flower-like architectures at different thicknesses in the 0.05–10.0 GHz range.

$$RL = 20 \log |(Z_{in} - Z_0) / (Z_{in} + Z_0)| \quad (2)$$

where f is the frequency of the electromagnetic wave, d is the thickness of an absorber, c is the velocity of light, Z_0 is the impedance of free space, and Z_{in} is the input impedance of absorber.

The RL values of the resin composites less than -20 dB, which is comparable to the 99% of EM wave absorption, were obtained in the 2.8–6.3 GHz range with absorber thickness of 2.6–5.0 mm as shown in Fig. 9. A minimum RL value of -48 dB was observed at 3.9 GHz with a matching thickness of 3.8 mm. Comparing with some other Ni hierarchical structures [18–22], the nickel flower-like architectures exhibited more efficient EM wave absorption (RL < -20 dB) in GHz range. The absorption characteristics can be understood as follows: as mentioned previously [57], the EM wave absorbing properties of magnetic materials, such as frequency, thickness, and absorbing band-width, are mainly determined by the frequency dependences of complex permittivity ($\epsilon_r' - j\epsilon_r''$) and permeability ($\mu_r' - j\mu_r''$). In this study, the complex permittivity of the resin composites with 20 vol% Ni flower-like architectures is low and almost independent of frequency indicating that dielectric loss can be neglected, and thus the EM wave absorbing properties strongly depend on the magnetic natural resonance (μ_r''). The μ_r'' exhibited higher value than other nickel nano/micro-structures [18–22], therefore, the Ni flower-like architectures exhibited more efficient EM wave absorption, which also suggested that there is a better electromagnetic matching of the complex permittivity and complex permeability. In addition, the 3D Ni flower-like architectures are composed of nanoflakes, therefore, such morphology induced the multi-scattering and repeated absorption of EM wave leading to more EM energy attenuation, which might be another factor for the EM wave absorption enhancement [20].

4. Conclusions

In conclusion, large scale monodispersed nickel flower-like architectures have been synthesized by a facile solvent-thermal process. The stepwise formation mechanism of the 3D flower-like architectures has been proposed including the nucleation of crystallites, the aggregation of initial nanoparticles, the oriented growth of nanoflakes along crystallographically specific direction and the Ostwald ripening. The experimental results indicated that sodium alkali, PEG, and NaCl played the important roles in the formation of final morphology feature. The as-obtained Ni architectures showed high coercivity of 332.3 Oe and saturation magnetization (M_s) of 47.7 emu/g. The resin composites with

20 vol% Ni flower-like powders showed efficient EM wave absorption characteristics (RL < -20 dB) in the 2.8–6.3 GHz range. Comparing with some other Ni hierarchical structures, the nickel flower-like architectures exhibited more efficient EM wave absorption in GHz mainly attributing to the flower-like structure composed of nanoflakes leading to large anisotropic field and repeated absorption of EM wave.

Acknowledgments

This work was supported by the grant for Qi-Lu Young Scholar program and Independent Innovation Foundations of Shandong University (2009JQ015, 2009TB010). The authors also acknowledge the financial supports from National Natural Science Foundation (21071090), the Research Fund for the Doctoral Program of Higher Education of China (20090131120032), the Excellent Young Scientist Fund of Shandong Province (BS2009CL040), the New Century Excellent Talent Program (NCET-10-0545), and the Returned Overseas Chinese Scholars, State Education Ministry.

Appendix A. Supporting materials

Supplementary data associated with this article can be found in the online version at doi:10.1016/j.jssc.2011.09.022.

References

- [1] A. Wolosiuk, O. Armagan, P.V. Braun, *J. Am. Chem. Soc.* 127 (2005) 16356.
- [2] L.X. Yang, Y.J. Zhu, H. Tong, Z.H. Liang, L. Li, L. Zhang, *J. Solid State Chem.* 180 (2007) 2095.
- [3] H.Q. Cao, G.Z. Wang, L. Zhang, Y. Liang, S.C. Zhang, X.R. Zhang, *Chem. Phys. Chem.* 7 (2006) 1897.
- [4] A. Butera, J.N. Zhou, J.A. Barnard, *J. Appl. Phys.* 87 (2000) 5627.
- [5] X.Y. Xu, Q.L. Wang, H.C. Choi, Y.H. Kim, *J. Membr. Sci.* 348 (2010) 231.
- [6] Y.P. Duan, J. Zhang, H. Jing, S.H. Liu, *J. Solid State Chem.* 184 (2011) 1165.
- [7] B. Zhang, X.C. Ye, W.Y. Hou, Y. Zhao, Y. Xie, *J. Phys. Chem. B* 110 (2006) 8978.
- [8] Y. Ren, L. Gao, *J. Am. Ceram. Soc.* 93 (2010) 3560.
- [9] P.R. Sajanlal, T. Pradeep, *J. Phys. Chem. C* 114 (2010) 16051.
- [10] P.P. Xiao, L.L. Zhu, Y.C. Zhu, Y.T. Qian, *J. Solid State Chem.* 184 (2011) 1459.
- [11] Q. Zhang, S.J. Liu, S.H. Yu, *J. Mater. Chem.* 19 (2009) 191.
- [12] L.P. Zhu, G.H. Liao, Y. Yang, H.M. Xiao, J.F. Wang, S.Y. Fu, *Nanoscale Res. Lett.* 4 (2009) 550.
- [13] L.J. Liu, J.G. Guan, W.D. Shi, Z.G. Sun, J.S. Zhao, *J. Phys. Chem. C* 114 (2010) 13565.
- [14] A. Narayanaswamy, H.F. Xu, N. Pradhan, X.G. Peng, *Angew. Chem. Int. Ed.* 45 (2006) 5361.
- [15] W.X. Zhang, C.B. Wang, H.L. Lien, *Catal. Today* 40 (1998) 387.
- [16] B. Kim, S.L. Tripp, A. Wei, *J. Am. Chem. Soc.* 123 (2001) 7955.
- [17] A.A. Zinchenko, K. Yoshikawa, D. Baigl, *Adv. Mater.* 17 (2005) 2820.
- [18] X.L. Dong, X.F. Zhang, H. Huang, F. Zuo, *Appl. Phys. Lett.* 92 (2008) 013127.
- [19] X.F. Zhang, X.L. Dong, H. Huang, Y.Y. Liu, W.N. Wang, X.G. Zhu, B. Lv, J.P. Lei, *Appl. Phys. Lett.* 89 (2006) 053115.
- [20] C. Wang, X. Han, P. Xu, J.Y. Wang, Y.C. Du, X.H. Wang, W. Qin, T. Zhang, *J. Phys. Chem. C* 114 (2010) 3196.
- [21] L. Qiao, X.H. Han, B. Gao, J.B. Wang, F.S. Wen, F.S. Li, *J. Appl. Phys.* 105 (2009) 053911.
- [22] P. Xu, X.J. Han, C. Wang, D.H. Zhou, Z.S. Lv, A.H. Wen, X.H. Wang, B. Zhang, *J. Phys. Chem. B* 112 (2008) 10443.
- [23] P. Toneguzzo, G. Viau, O. Acher, F. Fievet-Vincent, F. Fievet, *Adv. Mater.* 10 (1998) 1032.
- [24] B. Lu, H. Huang, X.L. Dong, X.F. Zhang, J.P. Lei, J.P. Sun, C. Dong, *J. Appl. Phys.* 104 (2008) 114313.
- [25] C.C. Lee, D.H. Chen, *Appl. Phys. Lett.* 90 (2007) 193102.
- [26] Z.G. An, S.L. Pan, J.J. Zhang, *J. Phys. Chem. C* 113 (2009) 2715.
- [27] S. Senapati, S.K. Srivastava, S.B. Singh, K. Biswas, *Cryst. Growth Des.* 10 (2010) 4068.
- [28] X.M. Ni, Q.B. Zhao, H.G. Zheng, B.B. Li, J.M. Song, D.E. Zhang, X.J. Zhang, *Eur. J. Inorg. Chem.* 23 (2005) 4788.
- [29] F. Ma, Q. Li, J.J. Huang, J.G. Li, *J. Cryst. Growth* 310 (2008) 3522.
- [30] X.M. Ni, Q.B. Zhao, D.E. Zhang, X.J. Zhang, H.G. Zheng, *J. Phys. Chem. C* 111 (2007) 601.
- [31] F.L. Jia, L.Z. Zhang, X.Y. Shang, Y. Yang, *Adv. Mater.* 20 (2008) 1050.
- [32] L.Y. Bai, J.M. Fan, Y.B. Cao, F.L. Yuan, A.H. Zuo, Q. Tang, *J. Cryst. Growth* 311 (2009) 2474.

- [33] J.G. Guan, L.J. Liu, L.L. Xu, Z.G. Sun, Y. Zhang, *Cryst. Eng. Commun.* 13 (2011) 2636.
- [34] F. Fievet, J.P. Lagier, M. Figlarz, *MRS Bull.* 14 (1989) 29.
- [35] Q.Y. Liu, X.H. Guo, J.L. Chen, J. Li, W. Song, W.J. Shen, *Nanotechnology* 19 (2008) 365608.
- [36] M. Niederberger, H. Colfen, *Phys. Chem. Chem. Phys.* 8 (2006) 3271.
- [37] G. Wulff, *Z. Kristallogr.* 34 (1901) 449.
- [38] M. Maillard, S. Giorgion, M.P. Pileni, *Adv. Mater.* 14 (2002) 1084.
- [39] X.W. Wei, X.M. Zhou, K.L. Wu, Y. Chen, *Cryst. Eng. Commun.* 13 (2011) 1328.
- [40] J. Lei, L. Xu, C. Morein, C.H. Chen, M. Lai, S. Dharmarathna, A. Doble, S.L. Suib, *Adv. Funct. Mater.* 22 (2010) 3373.
- [41] A.N. Kulak, P. Iddon, Y.T. Li, S.P. Armes, H. Colfen, O. Paris, R.M. Wilson, F.C. Meldrum, *J. Am. Chem. Soc.* 129 (2007) 3729.
- [42] A. Halder, N. Ravishankar, *Adv. Mater.* 19 (2007) 1854.
- [43] R.J. Joseyphus, T. Matsumoto, H. Takahashi, D. Kodama, K. Tohji, B. Jeyadevan, *J. Solid State Chem.* 180 (2007) 3008.
- [44] D. Ung, G. Viau, C. Ricolleau, F. Warmont, P. Gredin, F. Fievet, *Adv. Mater.* 17 (2005) 338.
- [45] E. Amstad, T. Gillich, I. Bilecka, M. Textor, E. Reimhult, *Nano Lett.* 9 (2009) 4042.
- [46] J. Zhao, D.W. Schaefer, *J. Phys. Chem. C* 112 (2008) 15306.
- [47] F. Xu, Y. Xie, X. Zhang, C.Z. Wu, W. Xi, J. Hong, X.B. Tian, *New J. Chem.* 27 (2003) 1331.
- [48] X.L. Wu, Y.G. Guo, L.J. Wan, C.W. Hu, *J. Phys. Chem. C* 112 (2008) 16824.
- [49] X. Wang, F.L. Yuan, P. Hu, L.J. Yu, L.Y. Bai, *J. Phys. Chem. C* 112 (2008) 8773.
- [50] X.A. Fan, J.G. Guan, Z.Z. Li, F.Z. Mou, G.X. Tong, W. Wang, *J. Mater. Chem.* 20 (2010) 1676.
- [51] T. Seto, H. Akinaga, F. Takano, K. Koga, T. Orii, M. Hirasawa, *J. Phys. Chem. B* 109 (2005) 13403.
- [52] C. Kittel, *Phys. Rev.* 73 (1948) 155.
- [53] L.J. Deng, P.H. Zhou, J.L. Xie, L. Zhang, *J. Appl. Phys.* 101 (2007) 103916.
- [54] F. Ma, Y. Qin, Y.Z. Li, *Appl. Phys. Lett.* 96 (2010) 202507.
- [55] J.R. Liu, M. Itoh, T. Horikawa, M. Itakura, N. Kuwano, K.I. Machida, *J. Phys. D: Appl. Phys.* 37 (2004) 2737.
- [56] T. Wang, J.P. He, J.H. Zhou, J. Tang, Y.X. Guo, X.C. Ding, S.C. Wu, J.Q. Zhao, *J. Solid State Chem.* 183 (2010) 2797.
- [57] J.R. Liu, M. Itoh, K.I. Machida, *Appl. Phys. Lett.* 83 (2003) 4017.